Fundamental Gridding-Related Dispersion Effects in Multiresolution Time-Domain Schemes

Costas D. Sarris and Linda P. B. Katehi, *Fellow, IEEE*

***Abstract*—The effect of electric and magnetic node arrangement on the dispersion characteristics of the multiresolution time-domain (MRTD) technique is investigated in this paper. It is first noted that, by adopting multiresolution analysis principles, the dispersion behavior of an arbitrary order MRTD scheme can be extracted from the analysis of the corresponding S-MRTD scheme, which is based on scaling functions only. Namely, the introduction of one wavelet level is expected to bring about a refinement in the resolution of S-MRTD by a factor of two. However, this contradicts several dispersion analyses of MRTD schemes that have been recently presented in the literature. This conflict between theoretical predictions and numerical observations is resolved through the proof that the introduction of wavelets does not result in the expected enhancement of resolution of an S-MRTD scheme, unless a certain arrangement of electric and magnetic field nodes is implemented.**

***Index Terms*—FDTD, MRTD, multiresolution analysis, numerical dispersion.**

I. Introduction

THE finite-difference time-domain (FDTD) technique offers a mathematically straightforward and inherently versatile method for the analysis of arbitrary electromagnetic geometries, at the expense of computational resources. Indeed, since Yee's scheme [1] is only second-order accurate and sensitive to numerical dispersion, a dense discretization of at least ten, but usually 25, points per wavelength is necessary for the extraction of a convergent solution. Therefore, the FDTD treatment of either electrically large geometries or fine detail structures typically results in a computationally intensive, memory and execution time-consuming calculation.

As an alternative to the conventional FDTD, several high-order numerical techniques have been developed [2] aimed at the discretization of electromagnetic structures at rates that may even approach the Nyquist limit. Furthermore, the incorporation of subgridding algorithms in the FDTD scheme [3] has demonstrated the potential of disconnecting the mean cell size within a domain from the size of the smallest geometric detail that is contained in the latter. Thus, a significant reduction in the computational cost, connected with the application of FDTD to complex geometries, appears to be attainable. Recently, wavelet-based time-domain methods (such as the the multiresolution time-domain (MRTD) technique) employing Battle–Lemarie, Daubechies, biorthogonal, and Haar wavelets were presented in [4]–[9] and references therein. Despite the fact that several techniques have been proposed for the mathematical derivation of these methods, in all cases, the introduction of one wavelet level in a numerical scheme formulated with scaling functions only (often referred to as S-MRTD), is expected to increase its effective resolution by a factor of two ("dyadic" property), as a direct consequence of multiresolution analysis (MRA) principles [10].

Nevertheless, dispersion analyses of several MRTD schemes have indicated that the addition of wavelets gives rise to phenomena that are not consistent with this expectation. In particular, the dispersion analysis of the Battle–Lemarie wavelet-based W-MRTD scheme that was carried out in [4] showed an only incremental improvement in its accuracy, compared to the corresponding S-MRTD scheme. This was accompanied by the observation of nonphysical modes that were attributed to spurious side effects of the use of wavelets. Moreover, a Haar MRTD dispersion analysis, presented in [7], led to the conclusion that almost no accuracy improvement was produced by the introduction of zeroth-order Haar wavelets to the corresponding S-MRTD scheme, which in this case coincided with FDTD. This conclusion agreed with the results of the relevant numerical study of [8] and provided the additional information that the effect of boundary conditions, which were supposed to be employed as a means of coupling wavelet coefficients to the excitation source [9], was actually negligible. Thus, it can safely be asserted that both Battle–Lemarie and Haar MRTD schemes under study in [4], [7], and [8] were formulated in a way that inherently prohibited the use of wavelets from resulting in a multiresolution analysis-consistent improvement of the dispersion properties of the underlying coarse grid scheme (this being either Battle–Lemarie-based S-MRTD or FDTD).

In this paper, the source of the aforementioned contradiction is investigated and the conditions under which MRTD schemes attain their expected dispersion properties are sought. Such a study is particularly important for the reason that a future direction of current wavelet research efforts is the development of microwave computer-aided design (CAD)-oriented algorithms. This motivates the assembly of theoretical tools that enable a reliable prediction of the accuracy properties of an MRTD type of scheme, for a given number of wavelet levels and an arbitrary basis. The current study is developed in three stages: Initially, the concept of equivalent grid points in an MRTD mesh is introduced. Then, the connection between the arrangement of electric and magnetic scaling functions in the mesh and the equivalent grid points that stem from the use of a certain number of wavelet levels is de-

Manuscript received March 30, 2001; revised August 24, 2001. This work was supported by the Army Research Office under the "Efficient Numerical Solutions to Large Scale Tactical Communication Problems" Project (DAAD19-00-1-0173).

The authors are with the Radiation Laboratory, Department of Electrical Engineering and Computer Science, The University of Michigan at Ann Arbor, Ann Arbor, MI 48109-2122 USA (e-mail: ksarris@umich.edu).

Publisher Item Identifier S 0018-9480(01)10471-0.

duced. Hence, a condition for the offset of electric and magnetic scaling functions in the mesh (which in FDTD equals half a cell) that need be imposed, for the equivalent grid points to be correctly positioned in the domain, is derived. Finally, a dispersion analysis based on a modified Fourier method recently introduced by the authors and briefly described in the Appendix, is used to confirm that the previous condition is sufficient for the achievement of the expected MRTD accuracy. This dispersion analysis is validated by a series of numerical experiments, whose results are shown to be in absolute agreement with it.

II. Electric and Magnetic Node Arrangement and Equivalent Grid Points in MRTD

In this section, MRTD is applied to the following system of two-dimensional (2-D) TE_z Maxwell's equations:

$$\frac{\partial E_y}{\partial t}(\overline{\rho},\, t) = \frac{1}{\epsilon}\left(\frac{\partial H_x}{\partial z}(\overline{\rho},\, t) - \frac{\partial H_z}{\partial x}(\overline{\rho},\, t)\right) \tag{1}$$

$$\frac{\partial H_x}{\partial t}(\overline{\rho},\, t) = \frac{1}{\mu}\frac{\partial E_y}{\partial z}(\overline{\rho},\, t) \tag{2}$$

$$\frac{\partial H_z}{\partial t}(\overline{\rho},\, t) = -\frac{1}{\mu}\frac{\partial E_y}{\partial x}(\overline{\rho},\, t) \tag{3}$$

with $\overline{\rho} = x\hat{x} + z\hat{z}$. Based on the method outlined in [4], update equations are derived by the method of moments, assuming a spatial expansion of electromagnetic field components in scaling and wavelet functions of an arbitrary basis and up to arbitrary orders $r_{x,\,\max,}$ and $r_{z,\,\max}$ in the x- and z-directions, respectively. However, our analysis is restricted to dyadic wavelet transforms, as they are the most commonly used for the purpose of adaptively solving partial differential equations. In the subsequent development, the discretization of a 2-D domain (in which field solutions are sought) in cells of Δx by Δz is pursued, by means of a wavelet basis, defined by the scaling function ϕ and the so-called mother wavelet ψ [10]. Then, $\phi_m(\xi) = \phi(\xi/\Delta\xi - m)$ denotes the mth scaling function in the $\xi = x,\, z$ direction. Accordingly, the wavelet functions of order r that recursively refine the resolution of ϕ_m are defined as : $\psi^r_{m,\,p} = 2^{r/2}\,\psi(2^r(x/\Delta x - m) - p)$, where $p = 0,\, \ldots,\, 2^r - 1$. A basis of pulse functions $h_n(t) = h(t/\Delta t - n)$ (defined as in [4]), is employed for field expansion in time, where Δt denotes the time step, limited by the choice of Δx and Δz through the stability condition. Given these definitions, E_y, H_x, H_z are expressed in the form of the following orthogonal expansions:

$$\begin{aligned} &E_y(\overline{\rho},\, t) \\ &\quad = \sum_n h_n(t) \sum_{i,\,m} \Bigg\{ {}_nE^{y,\,\phi\,\phi}_{i,\,m}\,\phi_i(x)\,\phi_m(z) \\ &\qquad + \sum_{r_z,\,p_z} {}_nE^{y,\,\phi\,\psi_{r_z,\,p_z}}_{i,\,m}\,\phi_i(x)\,\psi^{r_z}_{m,\,p_z}(z) \\ &\qquad + \sum_{r_x,\,p_x} {}_nE^{y,\,\psi_{r_x,\,p_x}\,\phi}_{i,\,m}\,\psi^{r_x}_{i,\,p_x}(x)\,\phi_m(z) \\ &\qquad + \sum_{r_x,\,p_x}\sum_{r_z,\,p_z} {}_nE^{y,\,\psi_{r_x,\,p_x}\,\psi_{r_z,\,p_z}}_{i,\,m} \\ &\qquad \times \psi^{r_x}_{i,\,p_x}(x)\,\psi^{r_z}_{m,\,p_z}(z)\Bigg\} \end{aligned} \tag{4}$$

$$\begin{aligned} &H_x(\overline{\rho},\, t) \\ &\quad = \sum_n h_{n'}(t) \sum_{i,\,m} \Bigg\{ n' H^{x,\,\phi\,\phi}_{i,\,m'}\,\phi_i(x)\,\phi_{m'}(z) \\ &\qquad + \sum_{r_z,\,p_z} n' H^{x,\,\phi\,\psi_{r_z,\,p_z}}_{i,\,m'}\,\phi_i(x)\,\psi^{r_z}_{m',\,p_z}(z) \\ &\qquad + \sum_{r_x,\,p_x} n' H^{x,\,\psi_{r_x,\,p_x}\,\phi}_{i,\,m'}\,\psi^{r_x}_{i,\,p_x}(x)\,\phi_{m'}(z) \\ &\qquad + \sum_{r_x,\,p_x}\sum_{r_z,\,p_z} n' H^{x,\,\psi_{r_x,\,p_x}\,\psi_{r_z,\,p_z}}_{i,\,m'} \\ &\qquad \times \psi^{r_x}_{i,\,p_x}(x)\,\psi^{r_z}_{m',\,p_z}(z)\Bigg\} \end{aligned} \tag{5}$$

$$\begin{aligned} &H_z(\overline{\rho},\, t) \\ &\quad = \sum_n h_{n'}(t) \sum_{i,\,m} \Bigg\{ n' H^{z,\,\phi\,\phi}_{i',\,m}\,\phi_{i'}(x)\,\phi_m(z) \\ &\qquad + \sum_{r_z,\,p_z} n' H^{z,\,\phi\,\psi_{r_z,\,p_z}}_{i',\,m}\,\phi_{i'}(x)\,\psi^{r_z}_{m,\,p_z}(z) \\ &\qquad + \sum_{r_x,\,p_x} n' H^{z,\,\psi_{r_x,\,p_x}\,\phi}_{i',\,m}\,\psi^{r_x}_{i',\,p_x}(x)\,\phi_m(z) \\ &\qquad + \sum_{r_x,\,p_x}\sum_{r_z,\,p_z} n' H^{z,\,\psi_{r_x,\,p_x}\,\psi_{r_z,\,p_z}}_{i',\,m} \\ &\qquad \times \psi^{r_x}_{i',\,p_x}(x)\,\psi^{r_z}_{m,\,p_z}(z)\Bigg\} \end{aligned} \tag{6}$$

where $n' = n + 1/2$, $i' = i + s_x$, and $m' = m + s_z$. Thus, while half a time step offset between the update of electric and magnetic field terms is kept (as in FDTD), the offset of electric and magnetic scaling cells in the x- and z-directions is left as a parameter under investigation. Most MRTD studies, with the notable exception of [11], adopt the choice of $s_x = s_z = 1/2$, based on the FDTD practice. In this paper, a systematic way of determining these offsets is set forth by introducing the notion of *equivalent MRTD grid points*.

Assume that a certain scaling function basis generates electric field grid points in one dimension ($\xi = x,\, z$): $i \cdot \Delta\xi$, $i = 1,\, 2,\, \ldots,\, N_\xi$. Then, the introduction of wavelets of orders $r = 0,\, 1,\, \ldots,\, r_{\xi,\,\max}$, refines the mesh in the ξ-direction by a factor of $\rho_\xi = 2^{r_{\xi,\,\max}+1}$, since each wavelet level successively doubles the resolution of the underlying approximation. In mathematical terms, the E_y expansion of (4) can be cast in the next equivalent form [10]

$$E_y(\overline{\rho},\, t) = \sum_n h_n(t) \sum_{i,\,m} \left\{ {}_nE^{y,\,\phi^{R_x}\,\phi^{R_z}}_{i,\,m}\,\phi^{R_x}_i(x)\,\phi^{R_z}_m(z)\right\} \tag{7}$$

where $R_x = r_{x,\,\max} + 1$, $R_z = r_{z,\,\max} + 1$, and $\{\phi^R_n(\xi)\} = \{2^{R/2}\phi(2^R(\xi/\Delta\xi) - n)\}$ is the scaling basis that produces by itself an approximation of the same resolution as (4). In fact, the latter corresponds to the hierarchical multiresolution decomposition of the former and the coefficients in (4) can directly be deduced from the ones in (7) via the wavelet transform. This wavelet-induced mesh refinement can also be perceived as a procedure of generating equivalent grid points that give rise to a mesh of cell sizes $\Delta x/\rho_x$, $\Delta z/\rho_z$. Similar observations hold for (5) and (6).

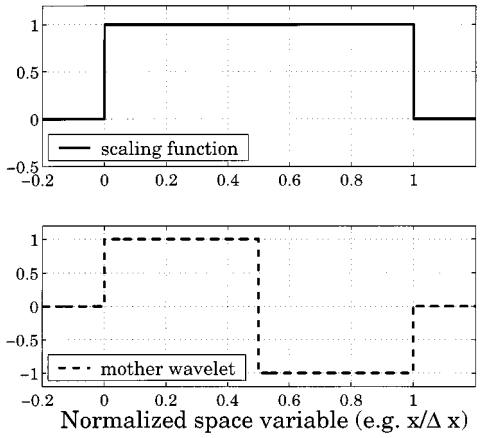

Fig. 1. Haar scaling and mother wavelet functions (space domain).

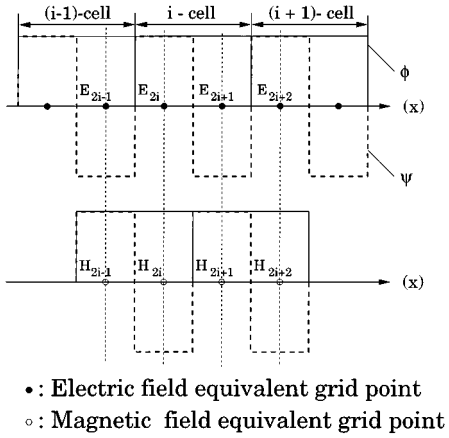

Fig. 2. Electric/magnetic field equivalent grid points for the zeroth-order Haar MRTD in one dimension, under formulation I.

This argument is demonstrated for a zeroth-order Haar MRTD scheme, utilizing Haar scaling and zeroth-order wavelet functions (Fig. 1), in Figs. 2 and 3, which depict the equivalent grid points that are generated, in both cases, in one dimension. It is noted that, in general, linear combinations of scaling and wavelet functions yield electric field values at points: $(i+(p+0.5)/2^{r_{x,\max}+1})\Delta x$, with $p = 0, 1 \cdots 2^{r_{x,\max}+1} - 1$. In our 2-D example, these figures represent *z-cuts* of the mesh, including E_y and H_z grid points (which are necessary for the approximation of x-partial derivatives involved in the E_y updates). Up to a normalization multiplicative constant, the field values at equivalent grid points within each cell are computed as the sum and the difference of scaling and zeroth-order wavelet terms, respectively. Accordingly, H_z equivalent grid points are located at $(i + s_x + (p + 0.5)/2^{r_{x,\max}+1})\Delta x$. However, the purpose of using wavelets is to implement in this "new" mesh of equivalent grid points the method produced by scaling functions only, at a resolution that is finer (in the x-direction) by the wavelet refinement factor ρ_x. Hence, if this method defines half a scaling cell offset between the electric and magnetic nodes, the wavelet augmented method has to define half an *equivalent* cell offset between the equivalent

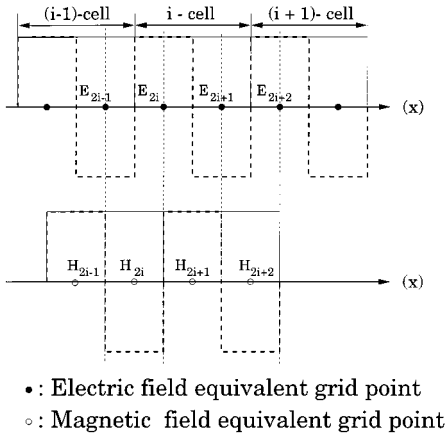

Fig. 3. Electric/magnetic field equivalent grid points for zeroth-order Haar MRTD in one dimension, under formulation II.

electric/magnetic grid points in this direction. The choice of s_x and s_z that is consistent with this requirement is as follows:

$$s_x = 0.5\rho_x = 2^{-r_{x,\max}-2}$$
$$s_z = 0.5\rho_z = 2^{-r_{z,\max}-2}. \tag{8}$$

Fig. 2 shows the node arrangement in the zeroth-order Haar MRTD, under the common convention of half a cell offset between electric/magnetic scaling cells, henceforth referred to as formulation I. Apparently, equivalent electric and magnetic equivalent nodes are now collocated. On the other hand, if the separation of electric and magnetic scaling cells is chosen in consistence with (8), which in this case yields an offset of one-quarter of a cell (Fig. 3), the equivalent grid points are leap-frogged in space and correctly correspond to the mesh of an FDTD scheme of cell size $\Delta x/2$. This approach will be hereafter referred to as formulation II.

Despite the fact that the electric/magnetic equivalent grid point collocation in formulation I was demonstrated for the Haar basis, its origin is the dyadic nature of the wavelet transforms under consideration, in the sense of the argument that was earlier developed. It is the purpose of the following dispersion analyses and numerical experiments to show that the difference in equivalent grids produced by formulations I and II results in different dispersion properties that render the former inconsistent while the latter consistent with MRA concepts.

III. Gridding Effect on the Accuracy of the Haar Wavelet-Based MRTD

A. Derivation of Arbitrary Order Haar MRTD Scheme

The relative simplicity of the Haar basis allows for the derivation and dispersion analysis of an arbitrary order scheme applied to (1)–(3). The update equations of the scheme are derived through the method of moments as in [4] and evaluating analytically the moment integrals pertinent to this technique. Field expansions of the type of (4)–(6) are assumed, where ϕ and ψ now denote the Haar scaling and mother wavelet functions, respectively (Fig. 1). In order to illustrate the difference between

formulations I and II, the form that the update equation of electric field scaling terms assumes in each one of them, is given below. In formulation I, this reads as

$$
\begin{aligned}
&{}_{n+1}E^{y,\,\phi\phi}_{i,\,m} \\
&\quad = {}_{n}E^{y,\,\phi\phi}_{i,\,m} + \frac{\Delta t}{\epsilon\Delta z}\Bigg\{ {}_{n'}H^{x,\,\phi\phi}_{i,\,m'} - {}_{n'}H^{x,\,\phi\phi}_{i,\,m'-1} \\
&\qquad\qquad + \sum_{1\le r\le r_{z,\,\max},\,p} \mathcal{C}(r,\,p)\Big({}_{n'}H^{x,\,\phi\psi_{r,\,p}}_{i,\,m'} \\
&\qquad\qquad\qquad - {}_{n'}H^{x,\,\phi\psi_{r,\,p}}_{i,\,m'-1}\Big)\Bigg\} \\
&\qquad - \frac{\Delta t}{\epsilon\Delta x}\Bigg\{ {}_{n'}H^{z,\,\phi\phi}_{i',\,m} - {}_{n'}H^{z,\,\phi\phi}_{i'-1,\,m} \\
&\qquad\qquad + \sum_{1\le r\le r_{x,\,\max},\,p} \mathcal{C}(r,\,p)\Big({}_{n'}H^{z,\,\psi_{r,\,p}\phi}_{i',\,m} \\
&\qquad\qquad\qquad - {}_{n'}H^{z,\,\psi_{r,\,p}\phi}_{i'-1,\,m}\Big)\Bigg\} \qquad (9)
\end{aligned}
$$

while in formulation II, it is modified as

$$
\begin{aligned}
&{}_{n+1}E^{y,\,\phi\phi}_{i,\,m} \\
&\quad = {}_{n}E^{y,\,\phi\phi}_{i,\,m} + \frac{\Delta t}{\epsilon\Delta z}\Bigg\{ {}_{n'}H^{x,\,\phi\phi}_{i,\,m'} - {}_{n'}H^{x,\,\phi\phi}_{i,\,m'-1} \\
&\qquad\qquad + \sum_{0\le r\le r_{z,\,\max}} 2^{r/2}\Big({}_{n'}H^{x,\,\phi\psi_{r,\,2^r-1}}_{i,\,m'-1} \\
&\qquad\qquad\qquad - {}_{n'}H^{x,\,\phi\psi_{r,\,2^r-1}}_{i,\,m'}\Big)\Bigg\} \\
&\qquad - \frac{\Delta t}{\epsilon\Delta x}\Bigg\{ {}_{n'}H^{z,\,\phi\phi}_{i',\,m} - {}_{n'}H^{z,\,\phi\phi}_{i'-1,\,m} \\
&\qquad\qquad + \sum_{0\le r\le r_{x,\,\max}} 2^{r/2}\Big({}_{n'}H^{z,\,\psi_{r,\,2^r-1}\phi}_{i',\,m} \\
&\qquad\qquad\qquad - {}_{n'}H^{z,\,\psi_{r,\,2^r-1}\phi}_{i',\,m}\Big)\Bigg\}. \qquad (10)
\end{aligned}
$$

In (9), $i' = i + 1/2$, $m' = m + 1/2$, and

$$\mathcal{C}(r,\,p) = 2^{r/2}\left(\delta_{p,\,2^{r-1}} - \delta_{p,\,2^{r-1}-1}\right)$$

where $\delta_{i,\,k}$ denotes Kronecker's delta function. In (10), $i' = i + 1/2^{r_{x,\,\max}+2}$ and $m' = m + 1/2^{r_{z,\,\max}+2}$. When $r_{x,\,\max} = r_{z,\,\max} = 0$, (9) shows that scaling and wavelet terms are de-coupled, which is consistent with the relevant observations in [7], [9]. This is not the case for (10) though, where scaling and wavelet terms are coupled for all MRTD orders. The same observations hold for the rest of the update equations that are similarly derived.

B. Stability and Dispersion Analysis

Implementing the modified Fourier method described in the Appendix, a dispersion analysis of arbitrary order Haar MRTD is carried out for both formulations I and II. Under the Fourier transform definition

$$\hat{f}(\lambda) = \int_{-\infty}^{+\infty} f(\mu)\, e^{j\lambda\mu}\, d\mu \qquad (11)$$

the Fourier transforms of Haar scaling and wavelet functions, with respect to a normalized wavenumber variable λ, are

$$
\begin{aligned}
\hat{\phi}(\lambda) &= \quad e^{j\lambda/2} \quad \frac{2}{\lambda} \quad \sin\frac{\lambda}{2} \\
\hat{\psi}(\lambda) &= -\ e^{j\lambda/2} \quad \frac{4j}{\lambda} \quad \sin^2\frac{\lambda}{4}.
\end{aligned} \qquad (12)
$$

Substituting these expressions into (44) of the Appendix leads to

$$
\begin{aligned}
&\mathcal{R}^{\psi_{r,\,p}}(\lambda) \\
&\quad = j\,2^{1+r/2}\exp\left(jp\lambda\left(\frac{1}{2} - \frac{3}{2^{r+1}}\right)\right)\frac{\sin^2\left(\lambda/2^{r+2}\right)}{\sin\left(\lambda/2\right)}. \qquad (13)
\end{aligned}
$$

Furthermore, the following substitutions are made into the finite-difference equations of the following two schemes:

$$
\begin{aligned}
{}_{n}E^{y,\,\phi\phi}_{i,\,m} &\rightarrow \hat{E}^{\phi\phi}_{y}\,\Lambda^{n}_{i,\,m} && (14)\\
{}_{n}E^{y,\,\phi\psi_{r,\,p}}_{i,\,m} &\rightarrow \mathcal{R}^{\psi_{r,\,p}}(-Z)\hat{E}^{\phi\phi}_{y}\,\Lambda^{n}_{i,\,m} && (15)\\
{}_{n}E^{y,\,\psi_{r,\,p}\phi}_{i,\,m} &\rightarrow \mathcal{R}^{\psi_{r,\,p}}(-X)\hat{E}^{\phi\phi}_{y}\,\Lambda^{n}_{i,\,m} && (16)\\
{}_{n}E^{y,\,\psi_{r,\,p}\psi_{r',\,p'}}_{i,\,m} &\rightarrow \mathcal{R}^{\psi_{r,\,p}}(-X)\mathcal{R}^{\psi_{r',\,p'}}(-Z)\hat{E}^{\phi\phi}_{y}\,\Lambda^{n}_{i,\,m} && (17)
\end{aligned}
$$

with

$$
\begin{aligned}
\Lambda^{n}_{i,\,m} &= e^{-j(\overline{k}_{\rho}\cdot\overline{\rho}_{i,\,m} + \omega n\Delta t)} && (18)\\
\overline{k}_{\rho} &= \hat{x}k_x + \hat{z}k_z \\
\overline{\rho}_{i,\,m} &= \hat{x}\,i\Delta x + \hat{z}\,m\Delta z && (19)
\end{aligned}
$$

and $X = k_x\Delta x$ and $Z = k_z\Delta z$. Similar substitutions are made for magnetic field components, taking into account the different conventions for electric/magnetic node separation. The condition that the resulting linear systems with respect to $\hat{E}^{\phi\phi}_{y}$, $\hat{H}^{\phi\phi}_{x}$, $\hat{H}^{\phi\phi}_{z}$ have nontrivial solutions yields the following dispersion relationships for formulations I and II, respectively:

$$
\begin{aligned}
\left\{\frac{1}{u_p\Delta t}\sin\frac{\omega\Delta t}{2}\right\}^2 &= \left\{\frac{1}{2\Delta x_{\text{eff}}}\sin\left(k_x\,\Delta x_{\text{eff}}\right)\right\}^2 \\
&\quad + \left\{\frac{1}{2\Delta z_{\text{eff}}}\sin\left(k_z\,\Delta z_{\text{eff}}\right)\right\}^2 \qquad (20)\\
\left\{\frac{1}{u_p\Delta t}\sin\frac{\omega\Delta t}{2}\right\}^2 &= \left\{\frac{1}{\Delta x_{\text{eff}}}\sin\frac{k_x\,\Delta x_{\text{eff}}}{2}\right\}^2 \\
&\quad + \left\{\frac{1}{\Delta z_{\text{eff}}}\sin\frac{k_z\,\Delta z_{\text{eff}}}{2}\right\}^2 \qquad (21)
\end{aligned}
$$

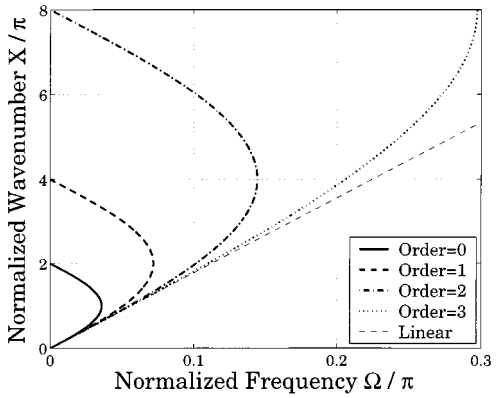

Fig. 4. Dispersion curves for propagation in (1,0) in Haar MRTD mesh (formulation I) of orders 0 to 3, $\nu = 0.05625$.

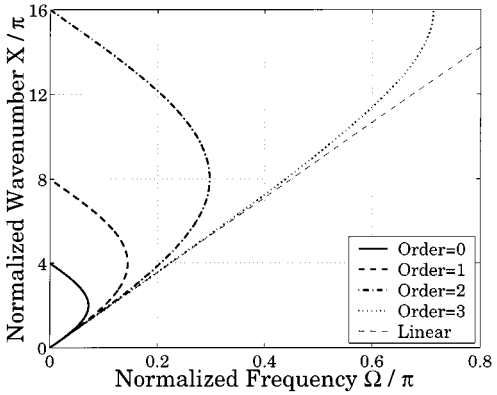

Fig. 5. Dispersion curves for propagation in (1,0) in Haar MRTD mesh (formulation II) of orders 0 to 3, $\nu = 0.05625$.

where $u_p = (\epsilon\mu)^{-1/2}$, $\Delta x_{\text{eff}} = \Delta x/\rho_x$, and $\Delta z_{\text{eff}} = \Delta z/\rho_z$. As proved in [12], the numerical scheme produced by means of a Haar scaling basis is FDTD itself, which can serve here as a measure of comparison for the accuracy of the two formulations under investigation. Indeed, comparing (20) and (21) with the respective formulas provided in [13], it is readily concluded that Haar MRTD under formulation I effectively implements an FDTD scheme of $2\Delta x_{\text{eff}} \times 2\Delta z_{\text{eff}}$ cell size, while Haar MRTD under formulation II attains an MRA consistent effective cell size of $\Delta x_{\text{eff}} \times \Delta z_{\text{eff}}$. This is graphically demonstrated in Figs. 4 and 5 that depict Haar MRTD dispersion curves for propagation in the direction $(1, 0)$ and value of the so-called Courant–Friedrichs–Lewy number $\nu = u_p\Delta t/\Delta x = 0.05625$. Moreover, the analytical dispersion relationship is plotted and denoted as "linear." It is thus shown that Haar MRTD under formulation I always finds itself one level of resolution (per direction) below the expected, while formulation II exhibits a consistent dispersion performance. In particular, for $r_{x,\max} = r_{z,\max} = 0$, (20) coincides with the dispersion relationship for FDTD of cell size $\Delta x \times \Delta z$ (which is the scaling cell size) and therefore it is concluded that the addition of zeroth-order wavelets does not improve the accuracy of Haar MRTD under formulation I (as a consequence of the fact that, in this case, scaling and wavelet update equations are uncoupled).

TABLE I
RESONANT FREQUENCIES (IN GHz) FOR THE 2-D CAVITY PROBLEM AND RELATIVE ERROR (DEGREES OF FREEDOM = 32 × 32)

(n,m)	$f_{n,m}$	MRTD form.I	R.E. (%)	MRTD form.II	R.E. (%)
(1,1)	0.6625	0.6624	-0.0109	0.6627	+0.0434
(2,1)	1.0474	1.0451	-0.2181	1.0466	-0.0809
(2,2)	1.3249	1.3233	-0.1194	1.3248	-0.0109
(3,1)	1.4813	1.4714	-0.6678	1.4786	-0.1825
(3,2)	1.6889	1.6827	-0.3673	1.6878	-0.0693
(3,3)	1.9874	1.9818	-0.2822	1.9861	-0.0652

Finally, stability criteria for the two formulations can be deduced from solvability conditions of (20) and (21) and assume the form

$$\Delta t \le \Delta t_I = \frac{2}{u_p\sqrt{\dfrac{1}{\Delta x_{\text{eff}}^2} + \dfrac{1}{\Delta z_{\text{eff}}^2}}} \tag{22}$$

$$\Delta t \le \Delta t_{II} = \frac{1}{u_p\sqrt{\dfrac{1}{\Delta x_{\text{eff}}^2} + \dfrac{1}{\Delta z_{\text{eff}}^2}}}. \tag{23}$$

C. Numerical Results

In order to numerically validate the results of the preceding dispersion analysis, FDTD and MRTD (formulations I and II) solutions for the $TE_{n,m}$ modes of a square air cavity structure of dimensions 32 cm × 32 cm are computed and compared. Haar MRTD schemes of orders 2 by 2, 3 by 3, and 4 by 4 (in x and z), corresponding to meshes of 4 × 4, 2 × 2, and 1 × 1 scaling cells are applied to the structure, along with a 32 × 32 cell FDTD. Hence, in all cases, the total number of degrees of freedom remains constant. Hard boundary conditions are modeled in MRTD by applying image theory for the update of magnetic field coefficients at the boundaries, as explained in [14]. Under these gridding conditions, our dispersion analysis predicts that FDTD and MRTD (formulation II) have the same accuracy, as they use the same number of degrees of freedom (thresholding is not applied in this study). This has been also numerically verified; the resonant frequencies that were extracted by FDTD and all MRTD schemes of formulation II, assume the *same* arithmetic values, some of which are given in Table I. On the contrary, formulation I shows a significantly worse accuracy, following that of an FDTD scheme of a 16 × 16 mesh. All simulations were performed at 0.9 of the stability limit for each scheme and frequency domain data were extracted from time domain data over 65 536 time steps. The numerical frequencies for all eigenmodes were found to agree well with their theoretical values, as predicted by (20) and (21). TE_{11} appears to be an exception for formulation II. Yet, in this case, the theoretical dispersion error [given by (21)] is −0.0076% and, therefore, numerical accuracy of the calculations clearly dominates phase errors in the final result. It is thus concluded that Haar MRTD under formulation II attains its expected resolution, just as the dispersion analysis showed and in contradiction to formulation I. Finally, the stable character of the proposed Haar MRTD formulation II is demonstrated by the electric field spatial distributions for TE_{22} and TE_{32} modes of the cavity, depicted in Figs. 6

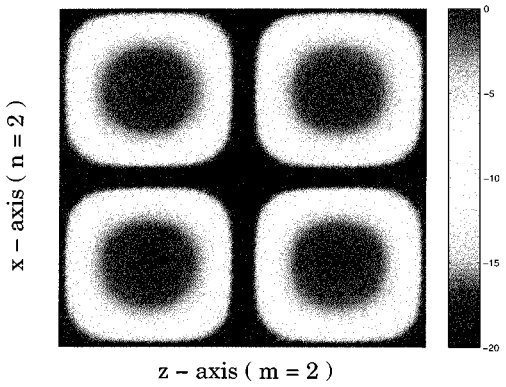

Fig. 6. Electric field distribution for TE_{22} mode obtained by an order 4 by 4 Haar MRTD (form. II), with a 1 by 1 scaling mesh.

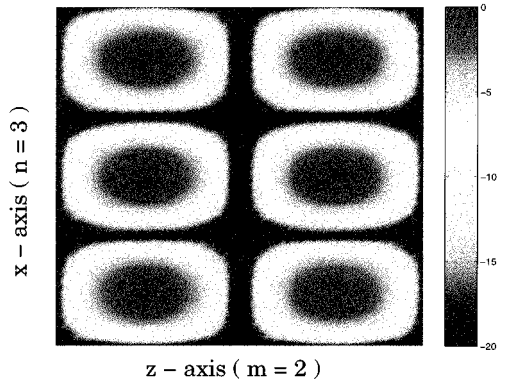

Fig. 7. Electric field distribution for TE_{32} mode obtained by an order 4 by 4 Haar MRTD (form. II), with a 1 by 1 scaling mesh.

and 7. Both modes were resolved by a 1×1 mesh of an order 4 by order 4 Haar MRTD (five wavelet levels per direction).

IV. Gridding Effect on the Accuracy of Battle–Lemarie Wavelet-Based MRTD

A. Derivation of W-MRTD Scheme

For the purpose of showing the generality of the gridding-related effects on the dispersion of MRTD that were pointed out for Haar-based schemes, the case study of a one-dimensional Battle–Lemarie wavelet-ased scheme (W-MRTD [4]) is presented in this section. In particular, the following system of Maxwell's equations is considered:

$$\frac{\partial}{\partial t} E_z(x, t) = \frac{1}{\epsilon} \frac{\partial}{\partial x} H_y(x, t) \tag{24}$$

$$\frac{\partial}{\partial t} H_y(x, t) = \frac{1}{\mu} \frac{\partial}{\partial x} E_z(x, t) \tag{25}$$

and discretized using Battle–Lemarie scaling and zeroth-order wavelet functions (Fig. 8) via the method of moments. Electric and magnetic field components are expanded in terms of the Battle–Lemarie basis as follows:

$$E_z(x, t) = \sum_{n, m} h_n(t) \Big\{ {}_n E_m^{z;\phi}\, \phi_m(x) + {}_n E_m^{z;\psi}\, \psi_m(x) \Big\} \tag{26}$$

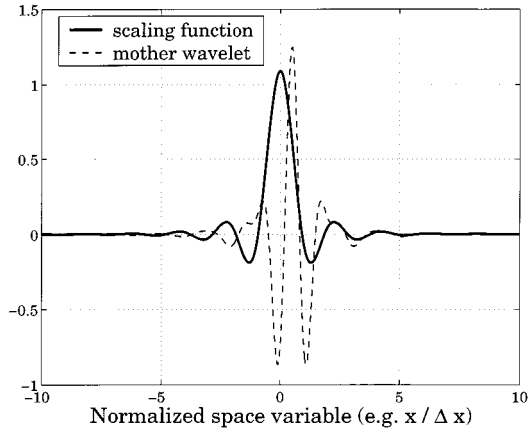

Fig. 8. Battle–Lemarie scaling and mother wavelet functions (space domain).

$$H_y(x, t) = \sum_{n, m} h_{n'}(t) \Big\{ {}_{n'} H_{m'}^{z;\phi}\, \phi_{m'}(x) + {}_{n'} H_{m'}^{z;\psi}\, \psi_m(x) \Big\} \tag{27}$$

with $n' = n + 1/2$, $m' = m + s$, and s is the electric/magnetic node offset that is again left as a parameter under investigation. The corresponding finite-difference equations assume the generic form

$$\begin{aligned} {}_{n+1} E_m^{z;\phi/\psi} = {}& {}_n E_m^{z;\phi/\psi} \\ & + \frac{\Delta t}{\epsilon \Delta x} \sum_p \alpha_E^{\phi/\psi}(p)\, {}_{n+(1/2)} H_{m+p+s}^{y;\phi} \\ & + \frac{\Delta t}{\epsilon \Delta x} \sum_p \beta_E^{\phi/\psi}(p)\, {}_{n+(1/2)} H_{m+p+s}^{y;\psi} \end{aligned} \tag{28}$$

$$\begin{aligned} {}_{n+1/2} H_{m+s}^{z;\phi/\psi} = {}& {}_{n+1/2} H_{m+s}^{z;\phi/\psi} \\ & + \frac{\Delta t}{\epsilon \Delta x} \sum_p \alpha_H^{\phi/\psi}(p)\, {}_{n+(1/2)} E_{m+p}^{y;\phi} \\ & + \frac{\Delta t}{\epsilon \Delta x} \sum_p \beta_H^{\phi/\psi}(p)\, {}_{n+(1/2)} E_{m+p}^{y;\psi} \end{aligned} \tag{29}$$

where the indicated summations extend over the "stencil" of the method. The stencil coefficients are computed by numerically evaluating integrals of Battle–Lemarie scaling and wavelet functions (in the spectral domain) that arise in the application of the method of moments for the derivation of (28) and (29). In particular, the explicit formulas for those read

$$\begin{aligned} & \alpha_E^{\phi}(p),\ \alpha_H^{\phi}(p) \\ & \quad = \int_{-\infty}^{+\infty} d\lambda \frac{\lambda}{\pi} |\hat{\phi}(\lambda)|^2 \sin(\lambda(p \pm s)) \end{aligned} \tag{30}$$

$$\begin{aligned} & \beta_E^{\phi}(p),\ \beta_H^{\phi}(p) \\ & \quad = \int_{-\infty}^{+\infty} d\lambda |\hat{\phi}(\lambda)||\hat{\psi}(\lambda)| \frac{\lambda}{\pi} \sin\left(\lambda\left(p + \frac{1}{2} \pm s\right)\right) \end{aligned} \tag{31}$$

$$\begin{aligned} & \alpha_E^{\psi}(p),\ \alpha_H^{\psi}(p) \\ & \quad = \int_{-\infty}^{+\infty} d\lambda |\hat{\phi}(\lambda)||\hat{\psi}(\lambda)| \frac{\lambda}{\pi} \sin\left(\lambda\left(p - \frac{1}{2} \pm s\right)\right) \end{aligned} \tag{32}$$

TABLE II
STENCIL COEFFICIENTS FOR THE W-MRTD SCHEME (FORMULATION II)

p	$\alpha_E^{\phi}(p)$	$\beta_E^{\phi}(p)$	$\beta_E^{\psi}(p)$
-8	+8.568e-03	+1.171e-02	-8.505e-03
-7	-1.601e-02	-2.187e-02	+1.622e-02
-6	+2.992e-02	+4.084e-02	-2.915e-02
-5	-5.596e-02	-7.607e-02	+5.864e-02
-4	+0.1051694	+0.1403895	-9.579e-02
-3	-0.2015483	-0.2474964	+0.2343052
-2	+0.4196303	+0.3727935	-0.3023901
-1	-1.3241406	-0.4279963	+1.9484456
0	+0.7974678	+0.3594450	+4.3699193
+1	+0.3590904	-0.2313141	-0.1205340
+2	-0.1816382	+0.1289039	+0.2431251
+3	+9.570e-02	-6.952e-02	-7.818e-02
+4	-5.103e-02	+3.728e-02	+5.605e-02
+5	+2.729e-02	-1.996e-02	-2.585e-02
+6	-1.461e-02	+1.069e-02	+1.502e-02
+7	+7.819e-03	-5.721e-03	-7.701e-03
+8	-4.185e-03	+3.062e-03	+4.219e-03

$$\beta_E^{\psi}(p),\ \beta_H^{\psi}(p) = \int_{-\infty}^{+\infty} d\lambda \frac{\lambda}{\pi} |\hat{\psi}(\lambda)|^2 \sin\left(\lambda(p \pm s)\right) \tag{33}$$

where $\hat{\phi}(\lambda)$ and $\hat{\psi}(\lambda)$ are provided in [4]. In [4], the parameter s is set equal to 1/2 (formulation I) and, thus, the apparent symmetries in the form of stencil coefficients (30)–(33) render the electric and magnetic field update equations dual. On the other hand, if, following formulation II and condition (8), s is set equal to 1/4, the only remaining symmetries are: $\alpha_E^{\psi}(p) = \beta_E^{\phi}(p-1)$ and $\alpha_H^{\psi}(p) = \beta_H^{\phi}(p-1)$. Some sample values of $\alpha_E^{\phi}(p)$, $\beta_E^{\phi}(p)$, and $\beta_E^{\psi}(p)$ are given in Table II. Their corresponding values under formulation I can be retrieved from [4].

B. Stability and Dispersion Analysis

A comparative stability and dispersion analysis of W-MRTD schemes under formulations I and II, according to the method described in the Appendix, leads to the following dispersion relationship:

$$\frac{4}{\nu^2}\sin^2(\Omega/2) = \left\{S_{\alpha_H^{\phi}} + \mathcal{R}^{\psi} S_{\beta_H^{\phi}}\right\}\left\{S_{\alpha_E^{\phi}} + \mathcal{R}^{\psi} S_{\beta_E^{\phi}}\right\} \tag{34}$$

where

$$S_q = \frac{1}{2j}\sum_p q(p)\, e^{jpX}$$

$$q = \alpha_E^{\phi},\ \alpha_H^{\phi},\ \beta_E^{\phi},\ \beta_H^{\phi} \tag{35}$$

$$\mathcal{R}^{\psi}(X) = \frac{\hat{\psi}(-X)}{\hat{\phi}(-X)} \tag{36}$$

and $\nu = u_p \Delta t/\Delta x$ and $\Omega = \omega\,\Delta t$, $X = k\,\Delta x$. The stability limit is numerically determined as the time step for which (34) yields complex frequency values that practically represent the transition of the numerical solution into the instability regime, in which it grows exponentially. In [15], the same calculation was based on the analytical derivation of lower bounds for the time step that guaranteed stability. However, one can easily verify numerically that these bounds are well below the actual Courant limit of W-MRTD and are therefore too restrictive.

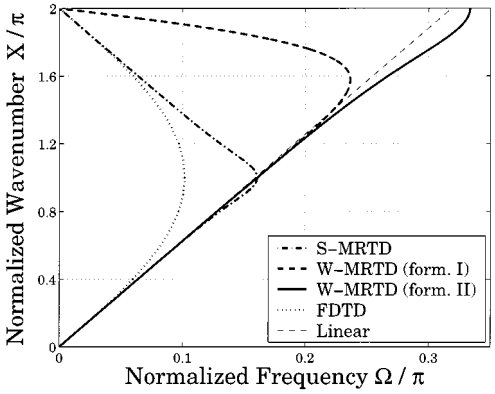

Fig. 9. Dispersion curves for W-MRTD (formulations I and II), S-MRTD, and FDTD.

Using the stencil coefficients of formulations I and II, (34) was employed to deduce the dispersion curves of the two schemes for $\nu = 0.15925$, and the range of p-index variation from $-p_0$ to p_0 and $p_0 = 9$. Both curves are depicted in Fig. 9. For comparison purposes, the dispersion curves of the so-called S-MRTD (utilizing Battle–Lemarie scaling functions only) and FDTD are also appended. As before, the analytical dispersion relationship is indicated as "linear."

Defining the turning point of the dispersion curve as the effective Nyquist limit of the corresponding scheme, it is observed that, for S-MRTD, this limit is $X = \pi$, for W-MRTD under formulation I it is $X \approx 1.6\pi$, while for W-MRTD under formulation II it is $X = 2\pi$, which shows that the former is inconsistent with MRA principles, while the latter does attain the expected refinement in resolution (compared to S-MRTD) by a factor of two. In fact, the dispersion curve of W-MRTD, formulation II can be readily extrapolated from the one of S-MRTD, by replacing X with $X/2$ in its expression.

This is also reflected in the stability condition for the two schemes. For S-MRTD, this condition is $\nu \leq 0.6371 = \nu_S$, for W-MRTD, formulation I, it becomes $\nu \leq 0.4384 = \nu_I$, and for W-MRTD, formulation II, $\nu \leq 0.3185 = \nu_{II}$. Hence,

$$\frac{\nu_S}{\nu_I} \approx 1.4534 \quad \frac{\nu_S}{\nu_{II}} \approx 2.0. \tag{37}$$

Thus, the previous conclusion is verified from a stability perspective: The addition of wavelets under the node arrangement of formulation I refines the scaling-based discretization by a factor of less than 1.5, while formulation II leads to a complete exploitation of the wavelets, doubling the resolution of S-MRTD.

It is noted that the results of our dispersion analysis of W-MRTD (formulation I) are consistent with those of [4], except for the fact that in [4] the dispersion diagram appears to consist of two branches, whence the claim that W-MRTD suffers from "spurious modes" was supported. However, as discussed in [16], our single branch diagram completely describes W-MRTD dispersion. With regards to the origin of modes that were observed in numerical experiments of [4] and were misconstrued as spurious (being attributed to

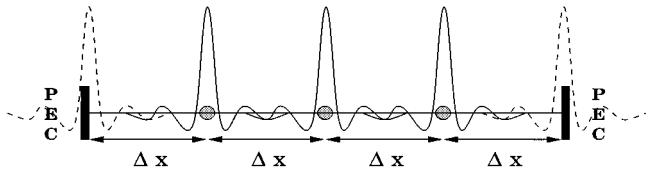

Fig. 10. W-MRTD computational domain for the 1-D cavity case study.

TABLE III
RESONANT FREQUENCIES (IN GHz) FOR THE 1-D CAVITY PROBLEM AND RELATIVE ERROR FOR W-MRTD (I, II)

$\frac{X_n}{\pi}$	f_n	W-MRTD Form.I	R.E. (%)	W-MRTD Form.II	R.E. (%)
0.25	3.75	3.7526	+0.0693	3.7401	-0.2640
0.50	7.50	7.5355	+0.4733	7.4929	-0.0950
0.75	11.25	11.3746	+1.1076	11.2706	+0.1831
1.00	15.00	15.3050	+2.0333	15.1276	+0.8507
1.25	18.75	19.2449	+2.6395	19.0716	+1.7152
1.50	22.50	22.4765	-0.1044	23.2963	+3.5391
1.75	26.25	19.8284	-24.4632	28.1173	+7.1135

the second branch of the dispersion diagram), it was shown to be the fact that the effective Nyquist limit of this scheme lay within the spectral support of the Battle–Lemarie wavelet function. For this reason, whenever this function is part of the initial conditions, it excites alias frequencies (that are also well predicted by our dispersion analysis).

C. Numerical Results

A simple numerical experiment that validates the dispersion analysis of the two W-MRTD schemes is presented in this section. In particular, a four-cell computational domain defined by three interior and two boundary Battle–Lemarie scaling cells ($\Delta x = 1$ cm) terminated into hard boundary conditions (that are implemented by image theory) is solved as a one-dimensional (1-D) cavity (Fig. 10). Then, the resonant frequencies $f_n = 3.75n$ [GHz] of the cavity, corresponding to normalized wavenumbers $X_n = 0.25\pi n$, are numerically determined from time-domain data of 8192 time steps. For both schemes, a time step equal to 0.5 of their stability limit is used ($\Delta t = 7.310$ ps and $\Delta t = 5.312$ ps, respectively), for the results to be directly comparable. The stencil value p_0 is set equal to 9. The sum of a scaling and a wavelet function located in the middle of the domain is used as the initial condition. By inspection of the spectral form of Battle–Lemarie scaling and wavelet functions [4], it is readily concluded that this kind of excitation injects into the grid normalized wavenumbers X ranging from 0 to 2π.

The resonant frequencies for the first seven modes of the cavity, obtained by the two W-MRTD schemes under comparison, are listed in Table III. It is clearly shown that W-MRTD under formulation II is consistently more accurate than formulation I, except for wavenumbers around the effective Nyquist limit of the latter, where its error changes sign (as it reaches this limit) and therefore assumes values close to zero. However, from that point on, the accuracy difference between the two schemes becomes significant. For example, when $X = 1.75\pi$, formulation I yields an alias frequency, presenting a relative error of -24.4632%. It is noted that this frequency is a product of inaccuracy, not a spurious mode, as was previously misinterpreted

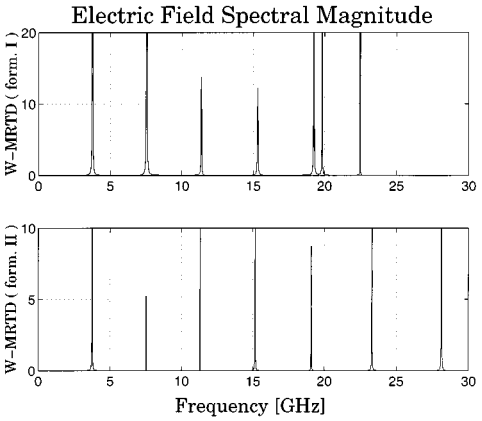

Fig. 11. Electric field spectral magnitude for the 1-D cavity problem, derived with W-MRTD under formulations I and II.

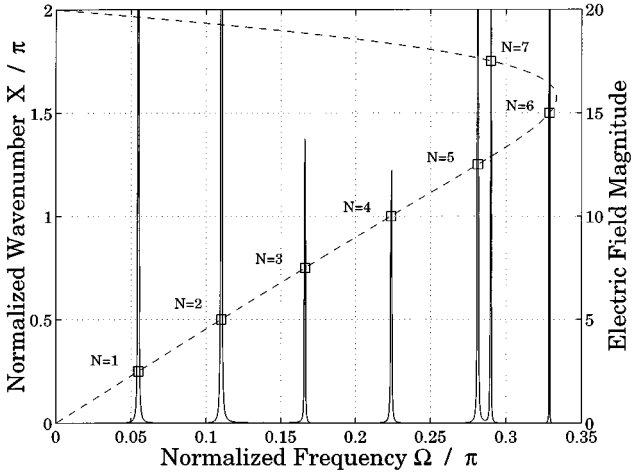

Fig. 12. Dispersion curve (- -) and electric field spectral magnitude (–) for the 1-D cavity case study with W-MRTD formulation I.

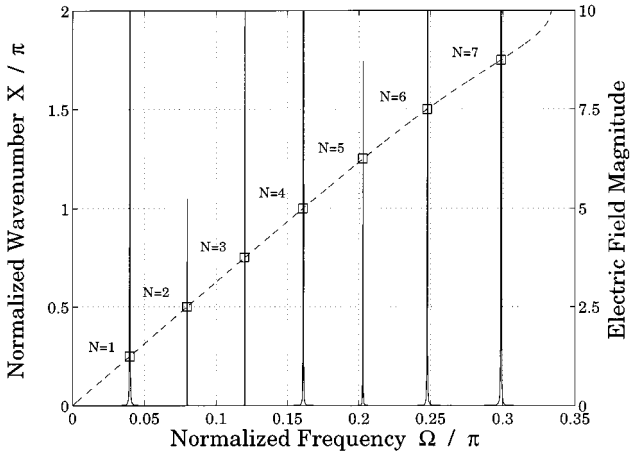

Fig. 13. Dispersion curve (- -) and electric field spectral magnitude (–) for the 1-D cavity case study with W-MRTD formulation II.

[4] and would appear in any scheme were that excited with wavenumbers above its Nyquist limit.

For the same geometry, numerical and theoretical results are presented and compared in Figs. 11–13. In particular, Fig. 11 depicts electric field spectral magnitudes derived by W-MRTD

under formulations I and II. Thus, the previously mentioned alias frequency, which corrupts the spectrum derived via formulation I, is clearly demonstrated, along with the ability of the second W-MRTD formulation to accurately resolve all cavity modes that are excited. In Figs. 12 and 13, the dispersion curves of the two W-MRTD schemes and the cavity field patterns that are deduced via their application, are jointly plotted. Square marks indicate the theoretical position of each of the seven modes on the dispersion curve of the corresponding scheme. The fact that, in all cases, the peaks of the electric field intersect the dispersion curve at the square marks, constitutes a numerical validation of our dispersion analysis. Furthermore, Fig. 12 provides an explanation of the way the "spurious" peak that appears in formulation I field pattern, is actually produced, as an alias frequency corresponding to the seventh cavity mode.

V. Conclusion

A necessary condition for the development of MRTD schemes with a consistent accuracy performance has been derived by means of dispersion analysis and confirmed by numerical experiments. It is also noted that, under the same condition, the two different methods of deriving wavelet schemes presented so far [4], [5] become equivalent. Thus, this work contributes to the fundamental understanding of the numerical properties of wavelet schemes and their connection to MRA principles, definitely resolving discrepancies and contradictions that existed in the MRTD literature for the last five years.

Appendix
The Modified Fourier Analysis Method for MRTD

For the purpose of formally performing a Fourier dispersion analysis of MRTD, the coefficients of electromagnetic field expansions in scaling and wavelet functions are first cast in the form of an inverse Fourier transform. For example, considering (4), one can use the well-known convolution theorem in order to transform the following expression [derived by means of the orthogonality properties of basis functions in (4)]:

$$ {}_nE_{i,m}^{y,\,\phi\,\phi} = \frac{1}{\Delta x\,\Delta z\,\Delta t}\int_{-\infty}^{+\infty} d\overline{\rho}\,dt\,E_y(\overline{\rho},\,t)\,\phi_i(x)\,\phi_m(z)\,h_n(t) \tag{38} $$

into the form

$$ {}_nE_{i,m}^{y,\,\phi\,\phi} = \frac{1}{8\pi^3}\int_{-\infty}^{+\infty} d\overline{k}_\rho\,dt\,e^{-j(\overline{k}_\rho\cdot\overline{\rho}_{i,\,m}+\omega n\Delta t)}\,\hat{E}^{y,\,\phi\phi} \tag{39} $$

with $\overline{k}_\rho$ and $\overline{\rho}_{i,\,m}$ as in (19), while

$$ \hat{E}_y^{\phi\phi} = \hat{E}_y\left(\overline{k}_\rho,\,\omega\right)\hat{\phi}(-k_x\,\Delta x)\,\hat{\phi}(-k_z\,\Delta z)\,\hat{h}(-\omega\,\Delta t) \tag{40} $$

and $\hat{E}_y(\overline{k}_\rho,\,\omega)$ is the spatio–temporal Fourier transform of $E_y(\overline{\rho},\,t)$. Moreover, $\hat{\phi}$ and $\hat{h}$ are Fourier transforms of scaling and pulse functions ϕ and h with respect to *normalized* variables $x/\Delta x$, $z/\Delta z$, and $t/\Delta t$, according to the definition of (11).

Following the same procedure, and after some trivial algebraic manipulations, scaling–wavelet, wavelet–scaling, and wavelet–wavelet coefficients can be cast in a similar form. In particular,

$$ {}_nE_{i,m}^{y,\,\phi\,\psi_{r,\,p}} = \frac{1}{8\pi^3}\int_{-\infty}^{+\infty} d\overline{k}_\rho\,dt\left\{e^{-j(\overline{k}_\rho\cdot\overline{\rho}_{i,\,m}+\omega n\Delta t)} \times\,\mathcal{R}^{\psi_{r,\,p}}(-k_z\,\Delta z)\,\hat{E}_y^{\phi\phi}\right\} \tag{41} $$

$$ {}_nE_{i,m}^{y,\,\psi_{r,\,p}\phi} = \frac{1}{8\pi^3}\int_{-\infty}^{+\infty} d\overline{k}_\rho\,dt\left\{e^{-j(\overline{k}_\rho\cdot\overline{\rho}_{i,\,m}+\omega n\Delta t)} \times\,\mathcal{R}^{\psi_{r,\,p}}(-k_x\,\Delta x)\,\hat{E}_y^{\phi\phi}\right\} \tag{42} $$

$$ {}_nE_{i,m}^{y,\,\psi_{r,\,p}\,\psi_{r',\,p'}} = \frac{1}{8\pi^3}\int_{-\infty}^{+\infty} d\overline{k}_\rho\,dt\left\{e^{-j(\overline{k}_\rho\cdot\overline{\rho}_{i,\,m}+\omega n\Delta t)}\mathcal{R}^{\psi_{r,\,p}}(-k_x\,\Delta x) \times\,\mathcal{R}^{\psi_{r',\,p'}}(-k_z\,\Delta z)\,\hat{E}_y^{\phi\phi}\right\} \tag{43} $$

where

$$ \mathcal{R}^{\psi_{r,\,p}}(X) = 2^{-r/2}\,e^{-jpX/2^r}\,\frac{\hat{\psi}(-X/2^r)}{\hat{\phi}(-X)}. \tag{44} $$

Magnetic field components are also transformed accordingly. Upon substitution of these expressions into MRTD finite-difference equations, a homogeneous linear system with respect to $\hat{E}_y^{\phi\phi}$, $\hat{H}_x^{\phi\phi}$, and $\hat{H}_z^{\phi\phi}$ is formulated (by equating the integrands of the previous Fourier integrals). If this system is written as

$$ \mathcal{A}\cdot\left[\hat{E}_y^{\phi\phi},\,\hat{H}_x^{\phi\phi},\,\hat{H}_z^{\phi\phi}\right]^T = 0 \tag{45} $$

the condition that it admits a nontrivial solution yields the MRTD dispersion relationship

$$ \det\mathcal{A}(\overline{k}_\rho,\,\omega) = 0. \tag{46} $$

Equivalently, one can directly substitute the kernels of the previous integral expressions into the finite-difference equations, as (14)–(17) imply. These kernels correspond to the well-known plane-wave type solutions that FDTD dispersion analysis employs.

It is worth noting that, no matter what the MRTD order is, the order of the system in (45) remains the same. The consistency of MRTD finite-difference equations and our Fourier analysis ensures that *any* three of the finite-difference equations being grouped as a linear system with respect to $\hat{E}_y^{\phi\phi}$, $\hat{H}_x^{\phi\phi}$, and $\hat{H}_z^{\phi\phi}$ lead to the same dispersion relationship. This greatly facilitates MRTD dispersion analysis that has so far been performed by faithfully following the FDTD dispersion analysis and without incorporating the multilevel character of the wavelet basis. For this reason, previous analysis approaches [4] would lead in this case to linear systems of $3\times 2^{r_{x,\,\max}+r_{z,\,\max}+2}$ unknowns ($r_{x,\,\max}$ and $r_{z,\,\max}$ being the maximum wavelet orders in x and z, respectively). A more detailed discussion on the modified Fourier analysis for MRTD schemes and its theoretical and numerical validation will be included in [17].

ACKNOWLEDGMENT

The research reported in this paper was initially inspired by a preprint of [11] that Prof. L. Carin, Duke University, Durham, NC, provided to the authors. This important contribution is gratefully acknowledged.

REFERENCES

[1] K. S. Yee, "Numerical solution of initial boundary value problems involving Maxwell's equations in isotropic media," *IEEE Trans. Antennas Propagat.*, vol. AP-14, pp. 302–307, Mar. 1966.

[2] A. Taflove, *Advances in Computational Electrodynamics: The Finite Difference Time Domain Method*. Norwood, MA: Artech House, 1998.

[3] I. S. Kim and W. J. R. Hoefer, "A local mesh refinement algorithm for the time domain finite difference method using Maxwell's curl equations," *IEEE Trans. Microwave Theory Tech.*, vol. 38, pp. 812–815, June 1990.

[4] M. Krumpholz and L. P. B. Katehi, "MRTD: New time domain schemes based on multiresolution analysis," *IEEE Trans. Microwave Theory Tech.*, vol. 44, pp. 555–561, Apr. 1996.

[5] W. Werthen and I. Wolff, "A novel wavelet based time domain simulation approach," *IEEE Microwave Guided Wave Lett.*, vol. 6, pp. 438–440, Dec. 1996.

[6] M. Aidam and P. Russer, "Application of biorthogonal B—Spline wavelets to Telegrapher's equations," in *Proc. 14th Annu. Rev. Progress Appl. Comput. Electromag.*, Monterey, CA, Mar. 1998, pp. 983–990.

[7] S. Grivet-Talocia, "On the accuracy of Haar-based multiresolution time domain schemes," *IEEE Microwave Guided Wave Lett.*, vol. 10, pp. 397–399, Oct. 2000.

[8] M. Fujii and W. J. R. Hoefer, "Numerical dispersion in Haar wavelet based MRTD scheme—Comparison between analytical and numerical results," in *Proc. 15th Annu. Rev. Progress App. Comput. Electromag.*, Monterey, CA, Mar. 1999, pp. 602–607.

[9] ——, "A three-dimensional Haar wavelet-based multi-resolution analysis similar to the 3-D FDTD method—Derivation and application," *IEEE Trans. Microwave Theory Tech.*, vol. 46, pp. 2463–2475, Dec. 1998.

[10] I. Daubechies, *Ten Lectures on Wavelets*. Philadelphia, PA: SIAM, 1992.

[11] T. Dogaru and L. Carin, "Application of multiresolution time domain schemes to two dimensional electromagnetic scattering problems," *IEEE Trans. Antennas Propagat.*, 1999, to be published.

[12] M. Krumpholz, C. Huber, and P. Russer, "A field theoretical comparison of FDTD and TLM," *IEEE Trans. Microwave Theory Tech.*, vol. 43, pp. 1935–1950, Sept. 1995.

[13] A. Taflove, Ed., *Computational Electrodynamics: The Finite Difference Time Domain Method*. Norwood, MA: Artech House, 1995, ch. 5: Numerical Dispersion.

[14] C. D. Sarris and L. P. B. Katehi, "Formulation and study of an arbitrary order Haar wavelet based MRTD technique," in *Proc. 16th Annu. Rev. Progress Appl. Comput. Electromag.*, vol. 2, Monterey, CA, Mar. 2000, pp. 540–547.

[15] E. M. Tentzeris, R. L. Robertson, J. F. Harvey, and L. P. B. Katehi, "Stability and dispersion analysis of Battle–Lemarie based MRTD schemes," *IEEE Trans. Microwave Theory Tech.*, vol. 47, pp. 1004–1013, July 1999.

[16] C. D. Sarris and L. P. B. Katehi, "On the existence of spurious modes in Battle–Lemarie based MRTD," *IEEE Microwave Wireless Comp. Lett.*, vol. 11, pp. 71–73, Feb. 2001.

[17] ——, "On the dispersion analysis of MRTD schemes," *IEEE Trans. Antennas Propagat.*, submitted for publication.

Costas D. Sarris received the Diploma degree in electrical and computer engineering (with distinction) from the National Technical University of Athens, Athens, Greece, in 1997, the M.S.E.E. degree from The University of Michigan at Ann Arbor, in 1998, and is currently working toward the Ph.D. degree at The University of Michigan at Ann Arbor, where he is involved with the field of time-domain analysis of microwave circuits and systems, utilizing wavelets.

Mr. Sarris was the recipient of four Hellenic Fellowship Foundation Prizes for the academic years 1993–1997, three Technical Chamber of Greece Awards for the academic years 1994–1997, all of them for scholastic achievement, and the 1997 NTUA/ECE Class Bronze Medal. He was also the recipient of a Student Paper Award (honorable mention) at the 2001 IEEE MTT-S International Microwave Symposium, Phoenix, AZ.

Linda P. B. Katehi (S'81–M'84–SM'89–F'95) received the B.S.E.E. degree from the National Technical University of Athens, Athens, Greece, in 1977, and the M.S.E.E. and Ph.D. degrees from the University of California at Los Angeles, in 1981 and 1984, respectively.

In September 1984, she joined the faculty of the Electrical Engineering and Computer Science Department, The University of Michigan at Ann Arbor, as an Assistant Professor, and then became an Associate Professor in 1989 and Professor in 1994. She has served in many administrative positions, including Director of Graduate Programs, College of Engineering (1995–1996), Elected Member of the College Executive Committee (1996–1998), Associate Dean For Graduate Education (1998–1999), and Associate Dean for Academic Affairs (since September 1999). She has authored or co-authored 410 papers published in refereed journals and symposia proceedings and she holds four U.S. patents. She has also generated 20 Ph.D. students.

Dr. Katehi is a member of the IEEE Antennas and Propagation Society (IEEE AP-S), the IEEE Microwave Theory and Techniques Society (IEEE MTT-S), Sigma Xi, Hybrid Microelectronics, and URSI Commission D. She was a member of the IEEE AP-S AdCom (1992–1995). She was an associate editor for the IEEE TRANSACTIONS ON MICROWAVE THEORY AND TECHNIQUES and the IEEE TRANSACTIONS ON ANTENNAS AND PROPAGATION. She was the recipient of the 1984 IEEE AP-S W. P. King (Best Paper Award for a Young Engineer), the 1985 IEEE AP-S S. A. Schelkunoff Award (Best Paper Award), the 1987 National Science Foundation Presidential Young Investigator Award, the 1987 URSI Booker Award, the 1994 Humboldt Research Award, the 1994 University of Michigan Faculty Recognition Award, the 1996 IEEE MTT-S Microwave Prize, the 1997 International Microelectronics and Packaging Society (IMAPS) Best Paper Award, and the 2000 IEEE Third Millennium Medal.